

Solar PV Module Parameter Extraction Using Sand Cat Optimization Technique

Karthik K¹, Ponnambalam P^{1*}

¹*School of Electrical Engineering Vellore Institute of Technology, Tamil Nadu, India*

Corresponding Author: Ponnambalam P

Abstract— This study explores a novel approach leveraging a cutting-edge meta-heuristic algorithm called Sand Cat Optimization. SCO draws inspiration from the hunting behavior of sand cats, mimicking their adeptness at navigating complex search spaces. The CEC 2019 benchmark test function's 20 most popular iterations serve as the foundation for the algorithm. It is contrasted with classical optimization algorithms. This bio-inspired algorithm is pitted against a range of established optimization techniques, including the conventional Newton-Rapson (NR) method and several evolutionary algorithms like Differential Evolution (DE), Generalized Opposition-Based Teaching and Learning-Based Optimization (GOTLBO), Ranking Teaching-Learning-Based Optimization (RTLBO), Gain-Sharing Knowledge-Based algorithms (GSK), and Teaching-Learning-Based Artificial Bee Colonies (TLABC). The measured and calculated data for SCO and the root mean square error values for all four PV models. The values for the single diode model (SDM), double diode model (DDM), STM6-40/36, and STP6-120/36 is $1.012 \times 10^{-16} \pm 2.17 \times 10^{-17}$, $1.7407 \times 10^{-16} \pm 3.77 \times 10^{-17}$, and $2.3626 \times 10^{-14} \pm 1.02 \times 10^{-16}$. It estimates the unknown parameters (I_{Ph}, I_D, R_s, R_{sh}, N₁) of a PV module using four well-known PV modules, the SDM/DDM, STM6120/36, and the STP6 40/36, under various normal operating circumstances. Regarding accuracy, the findings show that the suggested SCO algorithm is more efficient than previous optimization strategies. Sand cat Optimization (SCO) has the lowest root-mean-square error (RMSE), respectively. SCO consistently achieves remarkably low root mean square error values, indicating its exceptional accuracy in parameter estimation. This enhanced accuracy can be attributed to SCO's unique exploration and exploitation capabilities, allowing it to navigate the complex search space effectively and converge upon the optimal parameter set. The study employs Friedman's ranking and Wilcoxon tests to solidify the statistical robustness of the findings further.

Index Terms— Sand cat optimization (SCO); Single diode model; Swarm intelligence optimization; Metaheuristic algorithm; Root Mean Square Error (RMSE).

I. INTRODUCTION

Optimisation is crucial in various fields, including science, industry, and economics. It helps address complex challenges such as vehicle logistics, data source integration, vision tracking, constraint task scheduling, and NP-Hard problem-solving [1]. Parameter identification in photovoltaic models is a significant optimization problem that has garnered considerable attention from researchers [2]. Deterministic methods, such as curve fitting, iterative five-point methods, and analytical five-point methods, are commonly employed for this purpose, particularly for dual diode modules [3]. However, these methods require high accessibility and may not perform optimally under reduced solar radiation conditions. Meta-heuristic methods, such as Particle Swarm Optimization, have emerged as alternative approaches for PV model parameter estimation [4]. These methods offer advantages in handling

complex optimization problems and have shown promising results.

Evolutionary algorithms offer efficient solutions for non-linear implicit equations [5]. These population-based approaches leverage the collective intelligence of the entire population to find optimal solutions within a random search space [6]. Among EAs, genetic algorithms are widely recognized and applied [7]. While numerous metaheuristic algorithms exist, each with its strengths and limitations, their primary objective in photovoltaic applications is to optimize the physical parameters of PV modules [8]. Over the past decade, researchers have increasingly focused on developing real-time applications using bio-inspired and nature-inspired algorithms.

Metaheuristic approaches offer several advantages in optimization, including ease of use, flexibility, reduced processing time, and the ability to escape local optima in pursuit of global solutions. These characteristics make them particularly well-suited for tackling complex optimization problems. Inspired by the hunting behavior of sand cats, the Sand Cat Optimization algorithm leverages their exceptional digging skills and sensitivity to low-frequency sounds. The algorithm's two-phase approach, mimicking the sand cat's exploration and exploitation phases, enables efficient search space exploration while effectively converging towards optimal solutions. By optimizing the transition between these phases, SCO achieves superior results with fewer parameters and steps. Adaptive selection methods enhance the algorithm's performance [9].

The social interaction and movements of birds in nature motivated the partial swarm optimization. The algorithm searches for options to get the optimal solutions, using particles to identify possible solutions. Another method in this group is Ant Colony Optimization (ACO) [10]. Firefly Algorithm (FA) [11] Grey Wolf Optimization (GWO) [12], and Different Variance (DV) [13], Whale Optimization Algorithm (WOA) [14], Dragonfly Algorithm (DA) [15], Cuckoo Search (CS)[16], Butterfly Optimization Algorithm (BOA)[17] Wind-Driven Optimization (WDO) [18] Cat Swarm Optimization (CSO) [19] Fruit Fly Optimization Algorithm (FFOA). Inspired by sand cat hunting behaviour [20], the proposed algorithm demonstrates balanced exploration and exploitation capabilities due to its adaptive mechanism. Here are the key takeaways from this study:

1. Sand Cat Optimization is a novel population-based algorithm that mimics how sand cats search for and hunt prey.
2. SCO offers advantages over traditional algorithms. It requires fewer parameters, effectively avoids local optima, and exhibits balanced exploration and exploitation.

The article also mentions several studies related to parameter estimation in photovoltaic models.

- Studies using various optimization algorithms for parameter estimation of a three-diode PV model, Analytical and Sunflower Optimization Algorithm, Transient Search Optimization, Improved Marine Predators' Algorithm
- Studies focus on specific PV model parameter extraction algorithms: the Whale Optimization Algorithm, the Coyote Optimization Algorithm for a three-diode model [48–49], and Chaos Whale Optimization [50–52].

This paper's main contribution is as follows.

- To solve the solar PV parameter extraction problem, a new Meta-Heuristic (MH) optimization method (SCO) is introduced.
- For the SDM, DDM, STM6-40/36, and STP-120/36, the SCO recommended performance was successfully implemented, and it appears that the simulated and experimental I-V and P-V curves are exceptionally close.
- Comparisons are made between the results of the SCO and other Meta-Heuristic (MH) optimization methods.
- Considering the lowest Root Mean Square Error Objective, the proposed SCO was more desirable.

II. MODELING OF PV

Photovoltaic systems harness solar energy and convert it into usable electrical energy. This process involves converting sunlight into direct and alternating current using an inverter. PV systems can be classified into three main types: off-grid, grid-tied, and hybrid. Off-grid systems operate autonomously from the electrical grid and necessitate battery storage for continuous power supply. These systems suit televisions, phone signals, and street lighting applications.

On the other hand, grid-tied systems are directly connected to the electrical grid, allowing for immediate use or the sale of excess energy back to the grid. Hybrid systems combine features of both off-grid and grid-tied systems, incorporating battery storage alongside grid connectivity. Each type exhibits unique manufacturing processes, materials, costs, and performance characteristics. Silicon remains a prevalent material in solar cell production due to its wide availability and well-studied physical properties. Figure 1. highlights the importance of PV parameter extraction in understanding and enhancing the performance of photovoltaic systems. This technique utilizes mathematical models and optimization algorithms to determine the key characteristics of a solar cell or module.

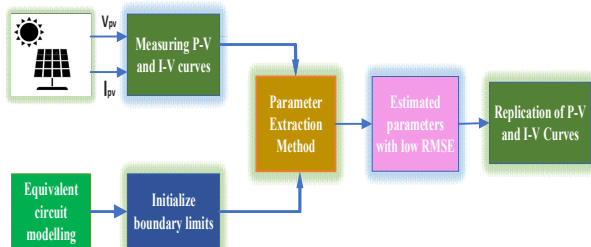


Figure 1. Block Diagram of PV Parameter Extraction

The process extracts the desired parameters by minimizing the difference between measured data and the model's predicted current-voltage curve. Monocrystalline silicon cells boast the highest efficiency (17%–25%) but come at a higher cost due to their production process, which uses more silicon. They also offer the longest lifespan and require the smallest area for a given power output. Polycrystalline silicon cells, while less efficient (12%–18%) due to multiple grain boundaries that increase recombination, are more cost-effective and simpler to manufacture. Amorphous thin-film cells, despite the efficiency advantages of crystalline silicon, are becoming increasingly affordable to produce.

Accurately modeling photovoltaic systems based on real-world current-voltage data is crucial for maximizing operational efficiency. However, external factors like temperature, air pressure, and irradiance fluctuations can significantly impact PV system performance. Even when manufacturers test modules under Standard Test Conditions (STC) 1000 W/m² irradiance, 25°C temperature, and 1.5 AM air mass - real-world efficiency may differ. This study extracts unknown parameters from the solar cell module by minimizing the difference between measured and predicted currents. This approach utilizes the root mean square error (RMSE), also known as root mean square deviation (RMSD), a statistical measure similar to standard deviation (SD), to quantify the model's accuracy.

A. Single Diode (DD) Model

The SD model is the most popular model for describing the electrical behaviour of a photovoltaic (PV) cell or model. This model simplifies the complicated physical behavior of the PV cell to a similar electrical circuit. The various parts of the single-diode model are as follows: Diode (D) series resistance (R_s), Shunt resistance (R_{sh}), and Current source (I_{ph}).

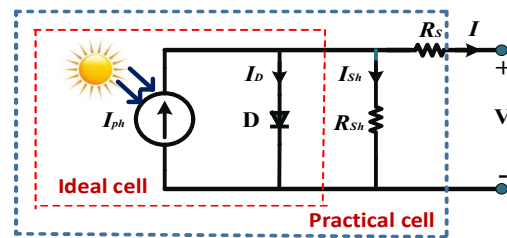


Figure 2. Single diode PV Model

$$I_L = I_{ph} - I_d - I_{sh} \tag{1}$$

$$I_L = I_{ph} - I_{Rd} \left[\exp \left(\frac{V_L + I_L R_s}{n V_t} \right) - 1 \right] \frac{V_L + I_L R_s}{R_{sh}} \tag{2}$$

Where I_{ph} , I_D , I_{Rd} and $R_{sh}E$ Represents the photo-generated current, diode current, reverse saturation diode current, and shunt resistor current, respectively. The identity factor of a diode is represented with n , and the series resistance is described with R_s and V_t Represents the junction thermal voltage. The Boltzmann constant, defined as k , is 1.3806503 10²³ J/K. The electron charge, q , equals 1.60217646 10¹⁹ C, and the temperature, T , is expressed in Kelvin. The I_L and V_L are the output voltage current and voltage, respectively. These represent measured data that the manufacturer has previously

determined, as well as the values of q , k , and T . Therefore, five unknown parameters (I_{ph} , I_{RD} , n , R_s , and R_{sh}) It needs to be calculated and optimized. Determining the parameters is difficult since they significantly affect the efficiency and reliability of the solar cell.

B. Double Diode (DD) Model

The double-diode model provides a more accurate representation of photovoltaic cell electrical behavior than the single-diode model, particularly under changing light and temperature conditions. This enhanced accuracy stems from incorporating an additional diode, accounting for recombination losses occurring within the depletion region and the bulk of the semiconductor material.

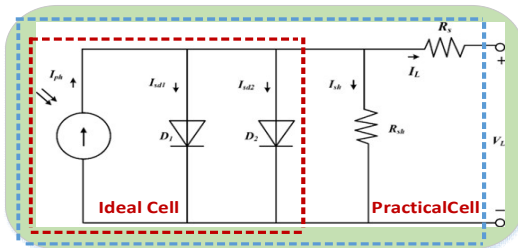


Figure 3. Equivalent double-diode PV Model circuit

$$I_L = I_{ph} - I_{d1} + I_{d2} - I_{sh} \tag{3}$$

Where I_{d1} is the First diode's current, and I_{d2} is the second Diode current

$$I_{D1} = I_{01} \left(\exp \left(\frac{V_L + I_L R_s}{n_1 V_t} \right) - 1 \right) \tag{4}$$

$$I_{D2} = I_{02} \left(\exp \left(\frac{V_L + I_L R_s}{n_2 V_t} \right) - 1 \right) \tag{5}$$

n_1 and n_2 are the first diode current, and I_{D2} is the second diode current.

$$I_L = I_{ph} - I_{RD1} \left(\exp \left(\frac{V_L + I_L R_s}{n_1 V_t} \right) - 1 \right) - I_{RD2} \left(\exp \left(\frac{V_L + I_L R_s}{n_2 V_t} \right) - 1 \right) - \frac{V_L + I_L R_s}{R_{sh}} \tag{6}$$

DD Model I-V curve with enhanced accuracy and parameter sensitivity. The DD model advanced analysis of PV Cell performance, particularly for high-precision applications, represents the first and second diodes' reverse saturation currents as I_{RD1} and I_{RD2} respectively, the ideal factors of the two diodes are n_1 and n_2 as follows: From equation 6, the seven unknown parameters, including I_{ph} , I_{RD1} , I_{RD2} , R_s , R_{sh} , n_1 , and n_2 of the PV systems.

C. Triple Diode (TD) Model

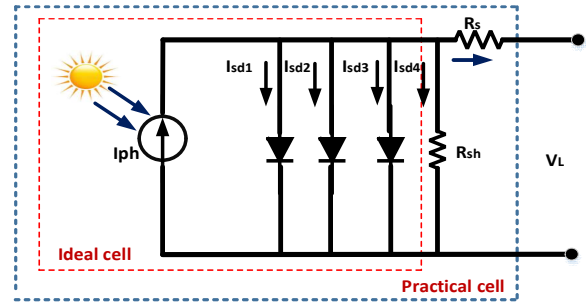


Figure 4. Equivalent Triple-diode modeling circuits

Figure 4 represents the schematic design of the TD model, which consists of a current source, a parallel pair of diodes, shunt resistance, and series resistance. The output current of the TD model is as follows, and equation 7 shows the output current of the TD model mathematically.

$$I_L = I_{ph} - I_{RD1} \left(\exp \left(\frac{V_L + I_L R_s}{n_1 V_t} \right) - 1 \right) - I_{RD2} \left(\exp \left(\frac{V_L + I_L R_s}{n_2 V_t} \right) - 1 \right) - I_{RD3} \left(\exp \left(\frac{V_L + I_L R_s}{n_3 V_t} \right) - 1 \right) - \frac{V_L + I_L R_s}{R_{sh}} \tag{7}$$

The first, second, and third diodes' reverse saturation currents are represented as I_{RD1} , I_{RD2} , and I_{RD3} respectively, the ideality factors of the three diodes are n_1 , n_2 and n_3 . Equation 7 includes the nine unknown parameters. I_{ph} , I_{RD} of the PV system.

D. N-number of diode model

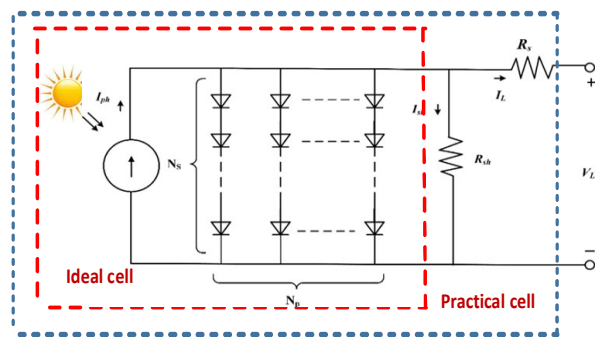


Figure 5. Equivalent N no of diode Model circuit

The equivalent circuit of the Photovoltaic (PV) module model is more complex because it includes more solar cells interconnected in series and parallels, as illustrated in Fig. 5.

$$I_L = N_p * I_{ph} - N_p I_{RD} \left(\exp \left(\frac{V_L + I_L R_s}{n_1 V_t} \right) - 1 \right) - \frac{V_L + I_L R_s N_s / N_p}{R_{sh} N_s / N_p} \tag{8}$$

From Equation 8, the five unknown parameters are I_{ph} , I_{RD} , n , R_s , R_{sh} . The number of solar cells linked in series is denoted by N_s , whereas the number of solar cells connected in parallel is denoted by N_p .

E. Objective Function

The root Mean Squared error (RMSE) is a commonly used objective function in regression analysis to measure the difference between predicted and observed values. It is the average squared difference between the predicted and observed values.

Mathematically, it is expressed as.

$$RMSE(X) = \sqrt{\frac{1}{N} \sum_{k=1}^N f(V_L, I_L, X)^2} \tag{9}$$

RMSE= Root Mean Square Error

N= No of measured data

X=Vector Solution

f(V_L, I_L, X) = The error Function

$$f_{SDM}(V_L, I_L, X) = I_{Ph} - I_{sd} \left(\exp\left(\frac{V_L + I_L R_S}{nV_t}\right) - 1 \right) - \frac{V_L + I_L R_S}{R_{sh}} - I_L \tag{10}$$

$$X_{SDM} = (I_{ph}, I_{sd}, n, R_s, \text{ and } R_{sh})$$

$$f_{DDM}(V_L, I_L, X) = I_{Ph} - I_{sd1} \left(\exp\left(\frac{V_L + I_L R_S}{n1V_t}\right) - 1 \right) - I_{sd2} \left(\exp\left(\frac{V_L + I_L R_S}{n2V_t}\right) - 1 \right) - \frac{V_L + I_L R_S}{R_{sh}} - I_L \tag{11}$$

$$X_{SDM} = (I_{ph}, I_{sd1}, I_{sd2}, n1, n2, R_s, \text{ and } R_{sh})$$

$$f_{PV Module}(V_L, I_L, X) = I_{Ph} N_p - I_{sd1} N_p \left(\exp\left(\frac{V_L + I_L R_S \frac{N_S}{N_P}}{n1V_t N_S} - 1 \right) \right) - \frac{V_L + I_L R_S \frac{N_S}{N_P}}{R_{sh} \frac{N_S}{N_P}} - I_L \tag{12}$$

$$X_{PV Module} = (I_{ph}, I_{sd}, n1, R_s, \text{ and } R_{sh})$$

III. SAND CAT OPTIMIZATION

A. Nature's Sand Cats: Inspiration

Sand cats are Felis. It inhabits stony and sandy deserts like the Sahara in Central Asia, the Arabian Peninsula, and Africa. Sand cats and domestic cats are physically different. Sand cats have sandy, pale grey hands and feet. Sand cats are 45–57 cm long. This method helps sand cats find subsurface parasites and rodents, as presented in Figure. 6. Sand and domestic cats have the same effect on the ear pinna flange. Sand cats have longer middle ear canals than domestic cats, creating more airspace. Sand cats may also identify noises by arrival time. Sand cats have a five-fold larger tympanic membrane than domestic cats, which affects their acoustic input admittance. Bone chains and middle ear cavities also increase acoustic input admittance. Scientific research shows that the sand cat's extraordinary emission frequency is below 2 kHz. Sand cats are 8 decibels more sensitive than domestic cats to this frequency. If its prey is underground, the curious sand cat may dig swiftly. Sand cats forage by searching and attacking.



a. Living

b. Searching behaviour for prey



c. Hunting prey

Figure 6. Behaviour of Sand cats

Additionally, a mechanism for fulfilling the exploration and exploitation stages and establishing optimal balance is given in the algorithm SCO. Sand and domestic cats have the same effect on the ear pinna flange. Sand cats have longer middle ear canals than domestic cats, creating more airspace.

Sand Cat Optimization draws inspiration from sand cats' hunting behaviors, specifically their exceptional ability to detect and capture prey. These solitary felines are remarkably adept at sensing low-frequency disturbances, allowing them to locate prey above and below ground. This unique skill inspired the development of the SCO algorithm. While sand cats are solitary creatures, the algorithm models them as a collective "herd" to leverage the principles of swarm intelligence for optimization. The number of "sand cats" within the algorithm can be adjusted to address minimization and maximization problems effectively. The problem must first be clearly defined to implement the SCO algorithm, then initializing the "sand cat" population. Each "sand cat" then explores the solution space, guided by low-frequency disturbance detection and swarm intelligence principles, to converge toward an optimal solution.

B. Exploration

As shown in Figure. 7, a sand cat is a $[1X]_d$ array that solves a d-dimensional optimal problem. A floating-point number (x₁, x₂, ..., x_d) represents each variable value. Each x must be between the lower and upper borders (∀x_i ∈ [lower, upper]). A candidate matrix containing the sand cat population according to the problem size Pop X N_d (pop=1..., n) is constructed before the SCO algorithm begins. The fitness function also determines each sand cat's fitness cost. The SCO uses this function to seek the optimal values for the problem's important parameters. A function will receive value from each sand cat. After an iteration, the sand cat with the lowest cost in the most recent iteration is selected as the best candidate for the best solution, and the other sand cats attempt to migrate towards it in the following iteration. The most favorable answer in each iteration may indicate the cat closest to its prey. A similar method efficiently uses memory by not keeping the solution for

that. If a better solution is found in the subsequent rounds, iteration in memory is performed.

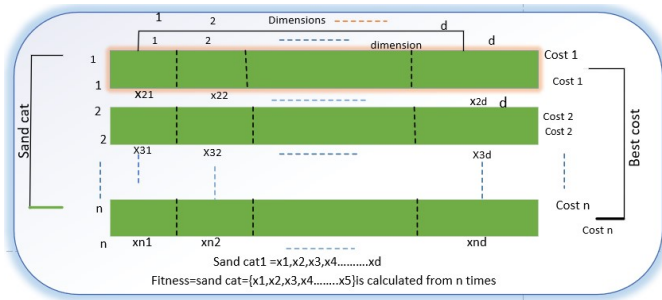


Figure 7. SCO's initialization and definition phase operational technique

$$\vec{r}_G = S_M - \left(\frac{2XS_M Xiter_c}{iter_{max} + iter_{max}} \right)$$

$$\vec{r}_G = 2 * \vec{r}_G \times rand(0,1). \vec{r}_G \quad (14)$$

$$r = \vec{r}_G \times rand(0,1) \quad (15)$$

Equation 14. The \vec{r}_G Early reductions from two to zero indicate the overall sensitivity range. In addition, \vec{r} the sensitivity range for each cat is shown. While the \vec{r}_G controls transition in these phases, \square They are used for exploration or exploitation actions. Iteration is the number of iterations that can be made, and $iter_c$ represents the current iteration.

$$\vec{P}_{os}(t+1) = \vec{r} (\vec{P}_{os_{bc}}(t) - rand(0,1) - \vec{P}_{os_c}(t)) \quad (16)$$

Based on the position of the best candidate ($\vec{P}_{os_{bc}}$), current position (\vec{P}_{os_c}), and sensitivity range (\vec{r}) Each search agent (sand cat) alters its location and other factors. Sand cat optimization can find other ideal prey spots—equation 16. The program may use this Equation to locate new local optima in the search space. The obtained position is in the middle of the current and prey locations. This is done using randomness rather than precision. Randomization helps the algorithm search agents, which simplifies and lowers running costs.

$$\vec{P}_{os_{ran}} = \left[rand(0,1) \cdot \vec{P}_{os_b(t)} \quad \vec{P}_{os_c(t)} \right] \vec{P}_{os}(t+1) \quad (17)$$

$$\vec{P}_{os}(t+1) = \left(\vec{P}_{os_b}(t) - \vec{r} \vec{P}_{os_{ma}} - \cos(\theta) \right) \quad (18)$$

As previously said, sand cats utilize their hearing to locate their prey. The space between the dunes distance between the optimal location of the sand cat ($\vec{P}_{os_{pr}}$) (best solution) and its current situation (\vec{P}_{os_c}) is computed using Equation. 17 to represent the attacking phase of SCO mathematically. Since the sensitivity range of sand cats is supposed to be circular, the movement direction is likewise determined by a random angle on the circle. Of course, additional factors stated in Equation 18 are also relevant when determining the movement's direction.

$$\vec{X}(t+1) = \begin{cases} \vec{P}_{os_b}(t) - P_{os_{ma}} \cdot \cos(\theta) \cdot \vec{r} & |R| < 1: \text{Exploitation} \\ \vec{r} \cdot \vec{P}_{os_{bc}}(t) + rand(0,1) \cdot \vec{P}_{os_c}(t) & |R| > 1: \text{Exploitation} \end{cases} \quad (19)$$

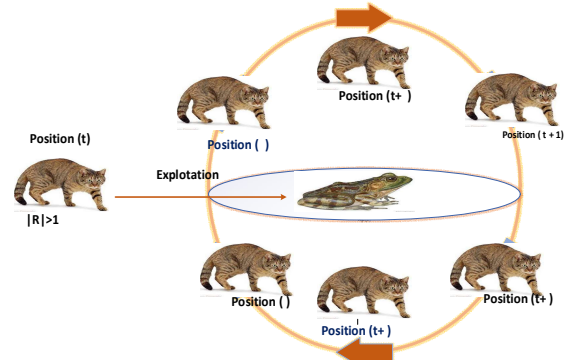


Figure 8. Prey attack (exploitation) versus prey search (exploire-ratio)

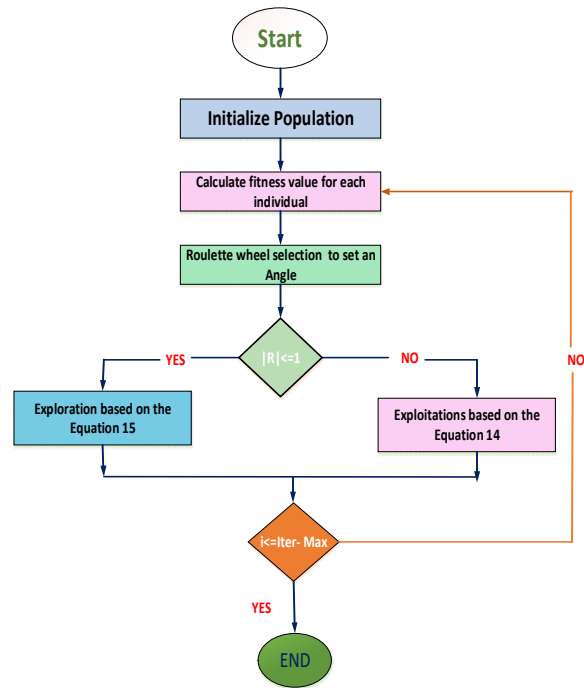


Figure 9. Flow chart for SCO algorithm

Figure 9 represents the fundamental principle of operation of the SCO method, which is to find the possible optimal solution from a random search space seeking prey and attacking them. Based on the problem, the algorithm's objective can be the minimum and maximum of an appropriate cost function. Based on this flowchart and the following steps, the optimal control parameter for the non-linear unstable system can be determined.

Algorithm 1 Sand cat Optimization for Pseudocode

```

// Initialize of the population
Initialize the population of solution
Calculate the fitness function of each individual in the population
Initialize the r, rc, R
While (t≤maximum iteration)
    For each individual search agent
// Update positions based on exploration and exploitation strategies
        Get a random angle based on the roulette wheel selection
        (0°≤θ≤360°)
        If (abs(R) ≤)
            New_position = exploration_strategy
        ELSE
            // Exploitation phase
            new_position = exploitation_strategy
        END IF
        // Bound check: Ensure the new position is within the search space
        new_position = bound_check(new_position)
// Evaluate the fitness of the new position
        new_fitness = evaluate_fitness(new_position)
// Update the position if the new position is better
        IF (new_fitness is better than current fitness), then
            Update position and fitness of individual i
        END IF
    END FOR
    // Select the best solutions (elitism or other selection strategies)
    best_solutions = select_best_solutions(population)
    // Optionally, perform additional operations (e.g., mutation)
    population = additional_operations(population)
END WHILE
// Output the best solution found
best_solution = get_best_solution(population)
Update the search agent position based on the eq.15
Else
    Update the search agent position based on the Eq.14 .
End
return best_solution
End
t=t++
End
    
```

ALGORITHM 1: Pseudocode for SCO

IV. PARAMETER RANGE OF THE PV SYSTEMS

Table 1 presents the lower bounds (L.B) and upper bounds (U.B) of each parameter (i.e., I_{ph} , I_{RD} , n , R_s , and R_{sh}) Or each Solar PV model, which is widely found in most of the previous studies [85]

TABLE 1 VARIOUS PV MODEL'S PARAMETER RANGES

Parameters	STM6-40/36		STP6-120/36		SD/DD Model	
	L.B	U. B	L.B	U. B	L.B	U. B
$I_{ph}(A)$	0	2	0	8	0	1
$I_{RD}(A)$	0	50	0	50	0	1
$R_s(\Omega)$	0	0.36	0	0.36	0	0.5
$R_{sh}(\Omega)$	0	1000	0	1500	0	100
$N_1 N_2$	1	60	1	50	1	2

The SD model is measured at 33°C and 1000 W/m² irradiance using 57 mm-diameter standard silicon RTC French cells. The STM6-40/36 module's 36 monocrystalline silicon cells are coupled in a series and operate at 51°C with 1000 W/m² irradiation. The 36 monocrystalline silicon cells of the STP6-120/36 module are linked in a series and operated at 55°C under 1000 W/m² irradiation.

TABLE 2 VARIOUS TRADITIONAL ALGORITHM PARAMETER SETTINGS

Algorithm	Parameter settings
SCO	NP = 26, kr = 0.9, kf = 0.5, K = 5
GSK	NP = 30, kr = 0.9, kf = 0.5, K = 10,
DE	NP = 30, F = 0.5, CR = 0.9
GOTLBO	NP = 50, Jr = 1.00
ITLBO	NP = 50
RTLBO	NP = 40
TLBO	NP = 30, TF = round (1 + rand (0,1))

Table 2 shows the search space for these model parameters. Additionally, there are six sophisticated artificial differential evolutions. (DE) Optimization methods and six fundamental metaheuristic algorithms are compared to the GSK algorithm (Storm and Price, 1997), teaching and learning-based optimization [72-74]. (TLBO) (Rao et al., 2011), grew oppositional educating and learning-based optimization (GOTLBO) (Chen et al., 2019), enhanced teaching and learning-based optimization (ITLBO) [75-78], ranking teaching and learning-based enhancement [79-82] (RTLBO) (Xiong et al., 2018a), and (TLABC) (Chen et al., 2018), improved whale IWOA (Xiong et al., 2018b) and In MATLAB 2021 b, each algorithm runs 30 times simultaneously.

Table 2, taken from each algorithm's original literature, shows the parameter settings for those algorithms [83],[84]. For different models, we set various Max_ values. The SDM's maximum is 50000, while the other PV models' maximums are 30000 and five parameters, respectively. The following subsection presents the comparison of various solar SD models (PW-201, STM6 40/36, and STP6-120/36) in terms of error, and also the Convergent curve, absolute current error (ACE), absolute power error (APE), I-V, and P-V curves of several solar SD models.

A. Comparison of general SD /DD Model with STM6 40/36 and STP6 120/36.

In this section, the comparison of various SD models is presented by taking the lower bounds LBs and upper bounds UBs value ranges of standard SD model parameters as a reference and are presented in Table 2 and. Here I_{ph} , I_D , R_s ,

P_{est} , N_L Are the unknown parameters of the standard SD model, and Table 3 depicts the estimated and measured values of power and current of the STM6 40/36 solar model along with the ACE, APE RMS error calculation, of where I_m & P_m and I_e & P_e Are the measured and estimated current and power, respectively? Figure 10 depicts error curves ACE and APE, and the convergence curves P-V and I-V depict the features of the STM6 40/36 solar model's measured and predicted value.

B. STM6 40/36 Solar Model

$$\sum_{i=1}^N |I_{L,est} - I_{L,mes}| = 0.069643$$

$$\sum_{i=1}^N |P_{L,est} - P_{L,mes}| = 0.0278$$

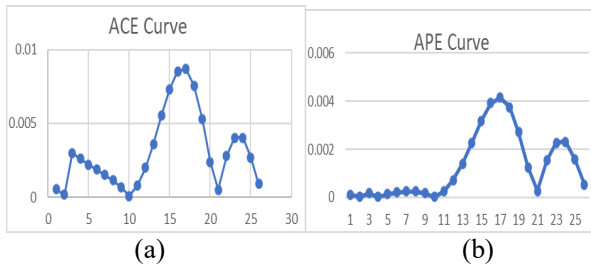


Figure 10 (a) ACE and (b) APE curve for STM6 40/36 model

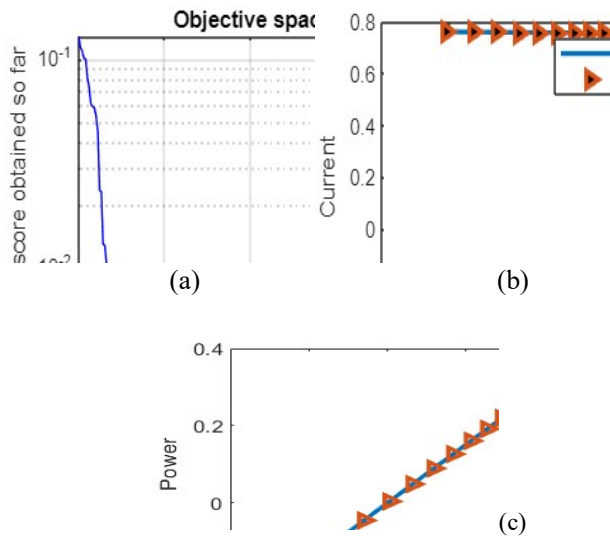


Figure 11(a). Convergence curve, (b) I-V curve, (c) P-V curve for measured and estimated values of STM6 40/36 model

Figure 11 Represents the convergence curve is a key tool for analyzing the performance of sand cat optimization algorithms. The chart progress of the optimization process typically shows the cost.

On the Y-axis and the number of iterations (optimization steps) on the X-axis. In general, the convergence curve for the SCO algorithm is used to decrease cost function value and rate of decrease compared with other algorithms.

C. STP6 120/36 Solar Model

Table 4 depicts the estimated and measured values of power and current of the STP6 120/36 solar model along with the ACE and APE RMS error calculation of where I_m & P_m and I_e

& P_e The measured and estimated current and power depict error curves ACE and APE and convergence curve, P-V, and I-V characteristics for measured and calculated values of STP6 120/36 solar models.

$$\sum_{i=1}^N |I_{L,est} - I_{L,mes}| = 0.271318$$

$$\sum_{i=1}^N |P_{L,est} - P_{L,mes}| = 3.868108$$

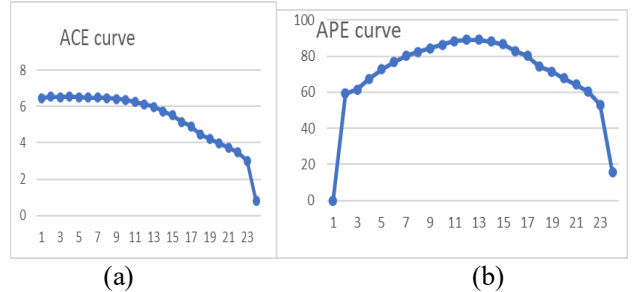


Figure 12. (a) ACE and (b) APE curve for STP6 120/36 Solar model

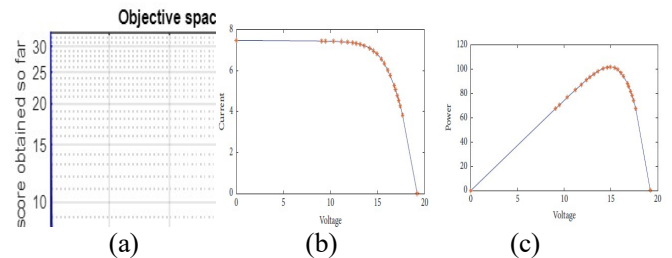


Figure 13. (a) Convergence Curve (b) I-V curve (c) P-V curve for measured and estimated values of STP6 120/36 solar model

Figure 13 (a) Convergence Curve specifically for the STP6 120/36 solar model optimized with SCO. In general, SCO to solar panel model parameter identification includes decreasing cost function value and rate of decrease compared with other algorithms. The Convergence curve shows how the optimization algorithm progresses toward finding the optimal set of parameters for the chosen SD model DD Model in the case of STP6 120/36. On the X-axis, typically see the number of iterations or function evaluations. In the Y-axis, you might see an error metric (e.g., Root Mean Square Error RMSE) between the measured I-V curve and the I-V curve predicted by the model with the current parameter set. A good convergence curve with minimal error and a close match between the measured and estimated curves in both I-V and P-V plots indicate successful parameter extraction.

D. Robustness of the SCO algorithm

a) SD/DD model

The SCO algorithm performs both approaches compared to the following popular algorithm. In objective functions, the SCO algorithm has shown outstanding performance. Similar values are given by the parameters determined using both methods. The current RMSE, determined using several STM6 40/36 panels, is 0.003303327. The RMSE is a current error, and STP6 120/36 is a solar panel at 735.7177. According to Friedman's test, the first approach's parameter estimation is superior to that of the second and third techniques. The comparison of various solar SD models (Standard SD model) is carried out in error terms

like (AC, AP, and RMS errors). Table 3 represents the comparison.

TABLE 3 COMPARISON OF DIFFERENT PANELS WITH SD/DD MODEL
REFERENCE MODEL

S.NO	Various Errors	STM6 40/36	STP6 120/36
1	AB error	0.069642896	128.1574
2	RMS error	0.003303327	735.7177
3	AP error	0.027816571	1683.844

b) STM6-40/36 model

The performance of both approaches, such as the SCO algorithm, is compared with the following modules. In objective functions, the SCO algorithm has shown outstanding performance. Similar values are given by the parameters determined using both methods. The current RMSE, determined using several STM64036 panels, is 0.00081. It is considered that the RMSE is a current error, and STP612036 is a solar panel at 482.286, which is given in Table 4. The Friedman test reveals that the first approach's parameter estimate is superior to the second and third strategies

TABLE 4 COMPARISON OF DIFFERENT PANELS WITH STM6-40/36 MODEL

S.NO	Various Errors	STM6 40/36	STP6 120/36
1	AB error	0.11933	103.5047
2	RMS error	0.000801	483.286
3	AP error	0.047615	1350.737

c) STP6-120/36 model

Friedman's test reveals that the first approach's parameter estimate outperformed the second and third techniques. The current RMSE, determined using several STM6 40/36 panels, is 0.000612, which is considered a current error. PWP201 is 0.02912, and STP6 120/36 is a solar panel at 0.007906. According to the Friedman test, the estimation parameter of the first approach is superior to that of the second and third techniques, as shown in Table 5.

Table 5 Different panels with STP6-120/36 model comparison

S.NO	Various Errors	STM6 40/36	STP6 120/36
1	AB error	0.09671	0.370941
2	RMS error	0.000612	0.007906
3	AP error	0.0448	5.211632

V. DISCUSSION

The SCO algorithm has performed exceptionally well in objective functions. The parameters obtained by the two approaches provide similar results. The current RMSE error with all four comparisons is displayed in Figure 14. The description compares the root mean squared error (RMSE) of three different solar panel models: STM6-40/36, STP120/36, and a single diode model. The main focus is likely on the RMS values for each model. Generally, a lower RMSE signifies a better fit between the solar panel model's predicted and actual power output. The STM6-40/36 panel has the lowest RMSE among the three, suggesting it offers the most accurate predictions compared to exact measurements. The RMS values depend on the operating conditions, particularly irradiance (sunlight intensity) and temperature levels, and they

represent an average across different situations. RMSE is a crucial metric, but factors like efficiency and each implementation might also be important. The choice of model would depend on the overall application requirements.

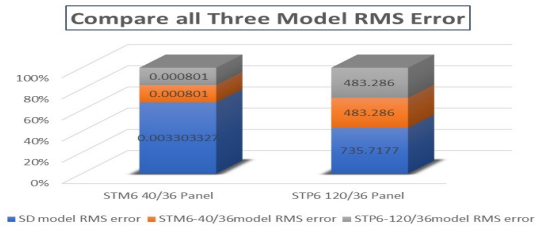


Figure 14. Compare all three modules with different panels. Each module is similar to a solar panel, but Figure 14 shows each has a different assessment. This method compares the performance of the SD, DD, STM6-40/36 model, and STP6-120/36 models under identical test conditions. The data collects performance metrics such as efficiency, power output, and degradation rates for each model and panel.

A. Individual absolute error (IAE)

a) IAE results for single diode module

Then, from Table 8, we choose five algorithms—GSK, DE, GOTLBO, RTLBO, and TLABC—with better RMSE values to compare with SCO. The calculated current data is obtained using these algorithms' retrieved parameters. By comparing the observed current with the estimated current of each method, the respective individual absolute error (IAE) values are determined and presented in Figure. 15. The method's IAE value is lower than those of other algorithms, suggesting that the algorithm has a greater SDM parameter extraction accuracy.

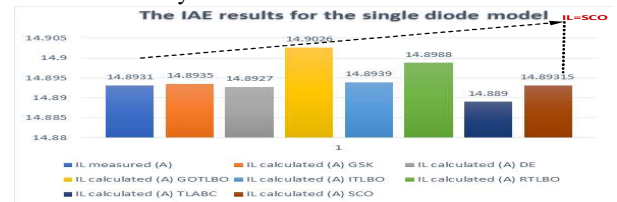


Figure 15. IAE results for the single-diode model

b) IAE results for the STM6-40/36 module

Then, we chose five algorithms—GSK, DE, GOTLBO, RTLBO, and TLABC—from Table 9 that have better RMSE values than SCO. These algorithms collect the parameters to create the calculated current data. Comparing the observed current with the estimated current of each method yields the relevant individual absolute error (IAE) values presented in Figure. 16. The algorithm's IAE value is lower than other algorithms, suggesting that it extracts parameters from the STM6-40/36 module more precisely.

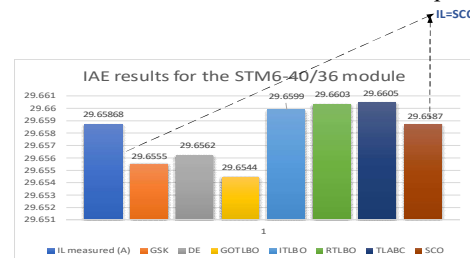


Figure 16. IAE results for the STM6/36 module

c) IAE results for the STP6-120/36

Then, we choose five algorithms—GSK, DE, GOTLBO, RTLBO, and TLABC—from Table 10 that have better RMSE values to compare with SCO. It contains the computed current data produced using the parameters that these methods extracted. Comparing the observed current with the estimated current of each method yields the relevant individual absolute error (IAE) values presented in Fig 13. The algorithm's IAE value is lower than other methods, demonstrating greater parameter extraction accuracy on the STP6-120/36 module.

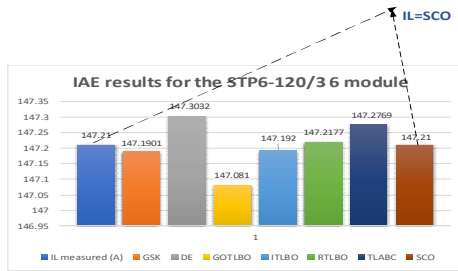


Figure 17. IAE results for the stp6-120/36 module

B. Parameter Calculations

Then, we choose five algorithms—GSK, DE, GOTLBO, RTLBO, and TLABC, respectively—with superior RMSE values than SCO. The algorithm's IAE value is lower than other algorithms, suggesting that it extracts parameters from the single diode module (SDM), PWP201 module, STP6-120/3 6 module, and STM6-40/36 module with more precision. The STP6-40/36 schematic below is growing better than other modules, as presented in Figure. 15. Increasing the number of iterations results in more precise output.

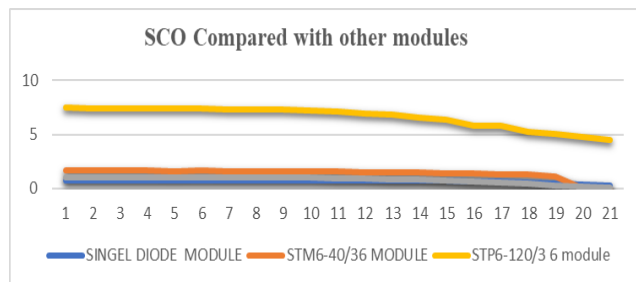


Figure 18. IAE results for SCO with other modules

Friedman's ranking test was also used to evaluate the competency and reliability of the deployed method. The CSO has the highest ranking, followed by the SDM, STM6-40/36, and STP6 120/36 modules. The STM6-40/36 is ranked top.

Friedman's ranking tests when you have multiple independent groups and want to compare the medians of those groups. Wilcoxon's signed-rank test, also known as the Wilcoxon matching-pairs signed-rank test, is a non-parametric statistical hypothesis test used to compare two related samples—
 Wilcoxon's signed-rank test when you have paired data and want to compare the medians of those pairs.

C. Comparison between different parameter extraction algorithms

a). Single diode model

When we use the available methods to obtain the SDM's parameters, the unknown parameters obtained are listed in Table 6. As demonstrated in Figure 19, the SDM rarely changes when parameter values obtained in various ways are applied.

TABLE 6 ESTIMATED PARAMETERS FOR SDM WITH SCO

Algorithm	Parameter	I_{ph} (A)	I_D (μ A)	R_s (Ω)	R_{sh} (Ω)	N
SCO		0.76025	0.32029	0.0360	53.00463	1.48393
GSK		0.7608	0.3231	0.0364	53.7227	1.4812
DE		0.7608	0.3231	0.0364	53.7185	1.4812
GOTLBO		0.7608	0.342	0.0362	53.8599	1.487
ITLBO		0.7608	0.323	0.0364	53.7187	1.4812
RTLBO		0.7608	0.3423	0.0361	55.3065	1.4871
TLABC		0.7608	0.3231	0.0364	53.7164	1.4812

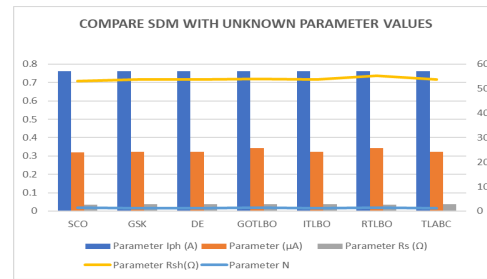


Figure 19. Parameters for SDM with Unknown Parameters

b). STP6-120/36 module

When we apply the algorithms mentioned to the parameter extraction of the SDM, the unknown extracted parameters of these algorithms are shown in Table 7. It can be seen that the parameter values extracted by these algorithms differ little in the STP6-120/36 module, as shown in Figure.

TABLE 7 ESTIMATED PARAMETERS FOR STP6-120/36 MODULE WITH SCO

Algorithm	Parameter	I_{ph} (A)	I_D (μ A)	R_s (Ω)	R_{sh} (Ω)	N
SCO		7.46	2.24	0.0026	22.5	1.2675
GSK		7.4725	2.335	0.0046	22.2199	1.2601
DE		7.4708	2.5614	0.0046	28.8094	1.2657
GOTLBO		7.4563	2.2559	0.0045	22.4749	1.2566
ITLBO		7.4725	2.335	0.0046	22.2199	1.2601
RTLBO		7.4728	2.3167	0.0046	21.6438	1.2594
TLABC		7.5611	3.4715	0.0049	23.6694	1.2698

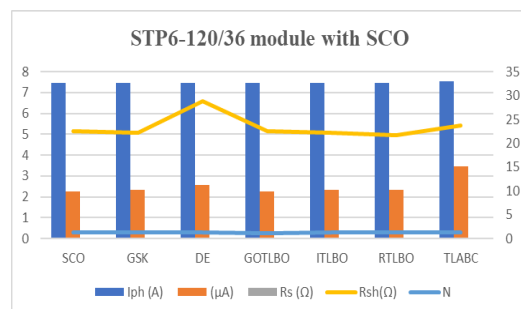


Figure 20. STP6-120/36 module with SCO

c). STM6-40/36 module

We have applied the techniques above to the SDM parameter extraction, and the unknown extracted parameters appear in Table 8. As shown in Fig. 17, the parameter values obtained by these methods varied only slightly in the STP6-40/36 module.

TABLE 8 ESTIMATED PARAMETERS FOR STM6-40/36 MODULE WITH SCO

Algorithm	Parameter				
	I_{ph} (A)	I_D (μ A)	R_s (Ω)	R_{sh} (Ω)	N
SCO	1.6629	2.3566	0.00245	16.546	1.53
GSK	1.6635	1.924	0.004	16.5546	1.5315
GOTLBO	1.6631	2.3475	0.0031	17.4323	1.5536
ITLBO	1.6639	1.761	0.0042	15.942	1.5217
RTLBO	1.6639	1.7024	0.0043	15.8288	1.518
BSA	1.6601	1.2069	0.0043	15.9283	1.5203
TLABC	1.7	1.6338	0.005	15.4001	1.5002

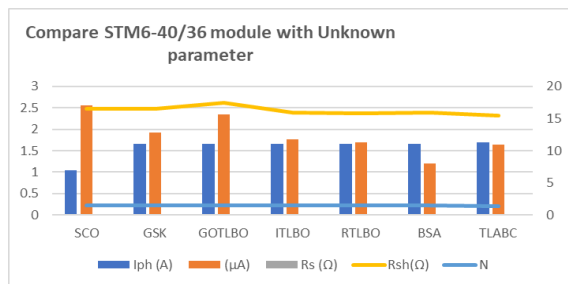


Figure 21. STM6-40/36 module with SCO

d). Comparison

Then, compared to SCO, we choose five algorithms: GSK, DE, GOTLBO, RTLBO, and TLABC. The technique's IAE value is less than that of other algorithms, indicating that the algorithm has a higher degree of precision of parameter extraction on the single diode module (SDM), STP6-120/36 module, and STM6-40/36 module. Fig 18 depicts the STP6-40/36 module outperforming the others. As the number of iterations rises, the outcome becomes more accurate.

TABLE 9 RANKED THE ALGORITHMS BASED ON FRIEDMAN'S RANK FOR SD/DD MODEL STM6-40/36, STP6-120/36, AND MODULES. R.T.C France Solar cell (SD/DDM) R.T.C France Solar cell (STM6-120/36) R.T.C France Solar cell (STM6-40/36)

Rank	Algorithm	Friedman's rank	Algorithm	Friedman's rank	Algorithm	Friedman's rank
1	CSO	1.835	CSO	1.7577	CSO	1.9908
2	GSK	6.8254	GSK	3.5595	GSK	3.2481
3	TLABC	7.0045	TLABC	6.6454	RTLBO	7.4800
4	DE	8.1431	RTLBO	7.9825	TLABC	7.4994
5	RTLBO	8.2552	GOTLBO	8.1024	DE	8.508
6	GOTLBO	9.9989	DE	8.7891	GOTLBO	8.7603

TABLE 10 COMPARISON OF RMSE VALUES WITH DIFFERENT ALGORITHMS FOR A SINGLE DIODE MODEL

Algorithm	RMSE			
	Best	Worst	Mean	Std
SCO	9.835E-04	1.856E-03	1.0120E-03	2.17E-04
GSK	9.8602E-04	9.8602E-04	9.8602E-04	2.18E-17
DE	9.8602E-04	1.3410E-03	1.0096E-03	6.72E-05
GOTLBO	9.8760E-04	1.7095E-03	1.0949E-03	1.36E-04
ITLBO	9.8760E-04	9.8602E-04	9.8602E-04	4.57E-17
RTLBO	9.8604E-04	1.0808E-03	1.0057E-03	3.06E-05
TLABC	9.8602E-04	1.0481E-03	9.9811E-04	1.76E-05

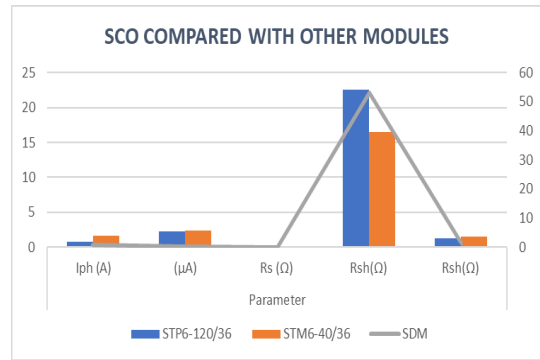


Figure 22. STM6-40/36 module with SCO

Friedman's scoring test can also be utilized to determine the ability and dependability of the adopted strategy. CSO has the highest ranking, followed by SDM/DDM, STM6-40/36, and STP6-120/36 modules. The STM6-40/36 is ranked top, as illustrated in Table 14

D. RMSE values of different algorithms

a). single diode model

SDM verifies the algorithm's performance by calculating the number of RMSE values (standard deviation, minimum, and maximum mean). Table 15 shows the experimental results of the six optimization strategies stated previously. In the event of a Max FE value of 30,000, it is worth noting that SCO has the smallest standard deviation (2.17E-04). The least significant RMSE (9.835E-04). In the parameter extraction of the single diode model, the SCO Algorithm is more competitive. In the early stages, it can be noticed that DE has a faster convergence speed than other algorithms. However, it quickly gets into the local optima. The SCO ultimately converges to the lowest RMSE value. Who demonstrates that the SCO algorithm improves the SDM's convergence performance

b). STM6-40/36 module

TABLE 11 COMPARISON OF RMSE VALUES WITH DIFFERENT ALGORITHMS FOR STM6-40/36 MODULE

Algorithm	RMSE			
	Best	Worst	Mean	Std
SCO	1.7398E-03	3.603E-03	1.7407E-03	3.77E-04
GSK	1.7298E-03	1.7298E-03	1.7398E-03	6.25E-18
DE	1.7738E-03	3.0774E-03	2.1503E-03	2.89E-04
GOTLBO	1.8467E-03	3.3823E-03	2.7718E-03	3.41E-04

ITLBO	1.7298E-03	1.9172E-03	1.7407E-03	3.47E-05
RTLBO	1.7298E-03	2.9934E-03	1.9041E-03	2.2900E-09
TLABC	1.7298E-03	2.4355E-03	2.0021E-03	2.04E-04

Computing several RMSE values (standard deviation, minimum, and maximum mean) confirms the STM6-40/36's performance technique. Table 16 shows the experimental outcomes of the six optimization strategies stated previously. In the event of a Max FE value of 30,000, SCO has the lowest standard deviation (3.77E-04). 1.7398E-03 is the lowest RMSE value. The SCO algorithm is superior in the parameter extraction of the single-diode model. DE has a faster convergence speed in the early stages than other algorithms. However, it swiftly slips into the local optima. The SCO ultimately converges to a lower RMSE value. This shows that the SCO algorithm outperforms the STM6-40/36 regarding convergence performance.

c). STP6-120/36 module

The technique's performance in STP6-120/36 is validated by calculating various RMSE values (standard deviation, minimum, and maximum mean). Table 17 displays the experimental results of the six optimization strategies stated above. In this instance of the Max FEs value of 30,000, it is worth noting that SCO has the smallest standard deviation (1.023E-04) and the least RMSE value (1.683E-02). The SCO Algorithm is more competitive in the parameter extraction of the single-diode model. It can be determined that DE has a faster convergence speed than other algorithms in its infancy. However, it quickly enters local optima. SCO ultimately converges on the lowest RMSE value.

As seen in Fig. 19, the SCO algorithm has higher convergence performance in the STP6-120/36 model gathering performance using established methods. For sand cat optimization algorithm to extract parameters for each model for simulation and data collection for each model. The best and the worst menace highest rank and worst menace lowest rank and mean rank menace average rank and standard deviation for computing. All compare the STM6-40/36 model, which performs better than others.

TABLE 12 COMPARISON OF RMSE VALUES WITH DIFFERENT ALGORITHMS FOR STP6-120/36MODULE

Algorithm	RMSE			
	Best	Worst	Mean	std
SCO	1.683E-02	1.68301E-02	2.36266E-02	1.02E-04
GSK	1.6601E-02	1.6601E-02	1.6601E-02	1.44E-16
DE	1.665E-02	3.4221E-02	2.228E-02	5.1E-03
GOTLBO	1.663E-02	3.0365E-02	2.151E-02	3.4E-03
ITLBO	1.661E-02	2.533E-02	1.7081E-02	1.77E-03
RTLBO	1.667E-02	2.079E-02	1.7031E-02	8.16E-04
TLABC	1.6701E-02	1.8988E-02	1.7271E-02	5.70E-04

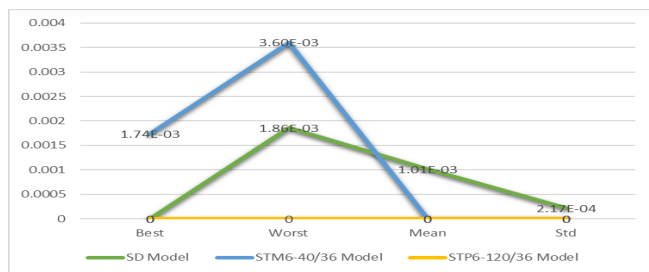


Figure 23. Ranking of SCO with another module

d) Comparison

Six better algorithms were chosen for comparison based on the RMSE values of the methods above in each PV module. We chose DE, GSK, DE, GOTLBO, RTLBO, ITLBO, and TLABC for the STM6-40/36 and STP6-120/36 modules. The computed current data acquired by these techniques is displayed in Tables 15, 16, and 17. The CSO Algorithm was successfully developed and implemented for parameter extraction of the Photowatt-PWP201 module for PV module designs, which has 36 polysilicon cells connected in series and irradiated to 1000 Wm² of radiation at 45 °C. Under 1000W/m² irradiance at 51 °C, The STM6-40/36 module's 36 monocrystalline silicon cells are interconnected in the series. Under 1000 W/m² irradiance at 55° C, the STP6-120/36 module's 36 monocrystalline silicon cells are linked in series.

For each algorithm's average execution time, The STMP6-40/36 Module and STP6 120/6 Module take significantly less time than the SMD module. Friedman's ranking test results are shown in Fig. 19. The average CPU time/sec best ranking obtained by the CSO, followed by the SMD module, is 3.14 s, indicating they are the most efficient in terms of computational speed STMP6-40/36 Module is 3.15 s slightly slower STP6 120/6 Module 3.176 s is somewhat longer than the other three models.

The average value of SCO is 3.15 s, and Fig.20 Represents SCO compared to all other five algorithms, i.e., GSK is 11 and DE is 31 s, GOTLBO is 32 s, RTLBO is 15 s, TLABC is 15 s, according to the Friedman ranking. SCO demonstrates significant efficiency compared to most other algorithms. While speed is crucial, it's important to consider other factors like accuracy and robustness when choosing an algorithm. Specific applications and their priorities will determine which algorithms are most suitable. The average CPU running time is less in SCO compared to the other five algorithms.

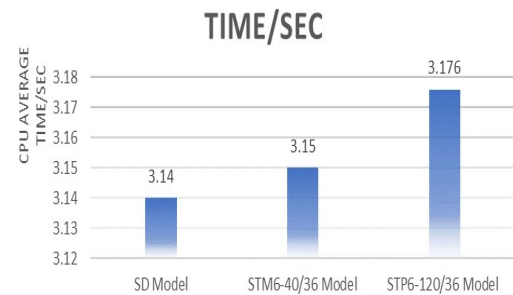


Figure 24. Comparison of the execution time of different modules.[85]

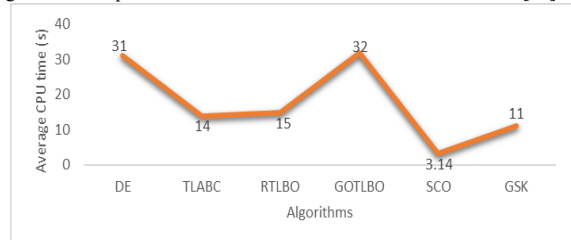


Figure 25. Ranking of SCO (Sand Cat optimization) and other compared algorithms on panel module according to the Friedman Test [85]

TABLE 13 RESULTS OF THE WILCOXON'S RANK SUM TEST FOR R.T.C FRANCE SOLAR CELL FOR STM6-40/36, STP6-120/36MODEL

R.T.C France Solar cell (SDM)					R.T.C France Solar cell (DDM)				
CSO	R ⁺	R ⁻	ρ Value	Result	CSO	R ⁺	R ⁻	ρ Value	Result
BES	46	0	3.0198X10 ⁻¹¹	+	BES	46	0	3.0199X10 ⁻¹¹	+
GSK	46	0	3.0086X10 ⁻¹¹	+	GSK	46	0	3.0199X10 ⁻¹¹	+
TLABC	46	0	3.0181X10 ⁻¹¹	+	TL ABC	46	0	3.0180X10 ⁻¹¹	+
DE	46	0	3.0129X10 ⁻¹¹	+	DE	46	0	3.0199X10 ⁻¹¹	+
RTLBOX	46	0	3.0180X10 ⁻¹¹	+	RTLBO	46	0	3.0199X10 ⁻¹¹	+
GOTLBO	46	0	3.0197X10 ⁻¹¹	+	GOTLBO	46	0	2.9543X10 ⁻¹¹	+

TABLE 14 RESULTS OF THE WILCOXON'S RANK SUM TEST FOR R.T.C FRANCE SOLAR CELL FOR SD/DD MODEL

R.T.C France Solar cell (STM6 40/36)					R.T.C France Solar cell (STP6 120/36)				
CSO	R+	R-	ρ Value	Result	CSO	R+	R-	ρ Value	Result
BES	464	0	2.2521X10-11	+	BES	464	0	2.8574X10-11	+
GSK	464	0	2.2362X10-11	+	GSK	464	0	1.9418X10-11	+
TLABC	464	0	2.8305X10-11	+	TLABC	464	0	2.8574X10-11	+
DE	464	0	2.8234X10-11	+	DE	464	0	2.8554X10-11	+
RTLBO	464	0	5.248X10-11	+	RTLBO	464	0	2.8556X10-11	+
GOTLBO	464	0	2.8287X10-11	+	GOTLBO	464	0	2.8574X10-11	+

Figure 21 demonstrates that the SCO algorithm significantly outperforms other algorithms, including Differential Evolution, Teaching-Learning-Based Optimization, Real-Time Learning-Based Optimization, Gradient-Opposition-Based TLBO, and Gaining-Sharing Knowledge-Based Optimization, in terms of execution time. This faster performance makes SCO a superior choice for applications where computational efficiency is critical. Statistical analysis using Wilcoxon's test, as summarized in Tables 17 and 18, further supports the superiority of SCO. The study reveals that SCO consistently outperforms the other metaheuristic algorithms in solving parameter estimation problems for five different solar PV cell/module models. Specifically, SCO achieves higher R+ values (indicating better performance) than R- values across all five models, highlighting its consistent advantage over traditional metaheuristic methods.

VI. CONCLUSION

In this research investigation, a well-known optimisation technique, known as the SCO optimization algorithm, is used to obtain the optimum solution for solar PV cells and module parameters. SCO was employed to estimate the SD/DD Model, STM6 40/36, and STP6 120/36 PV panel module parameters to show the performance of the SCO optimization algorithm. The calculated and estimated data's I-V characteristics, as well as P-V characteristics, demonstrated the suggested method's higher degree of accuracy. The simulation results test and comparisons to other metaheuristics optimisation techniques illustrate the method's accuracy and validity in extracting the characteristics of a PV cell and module. The SCO handles seven engineering design challenges: welded beam, compression springs, pressure vessels, piston levels, speed reduction, 3-bar truss, and cantilever beam. It observed the benefit of fast convergent and consistent results for each test. The approach uses the real world.[1]

information from several solar PV manufacturers (SD/DD Model, STM6-40/36, and STP6-120/36). The solar cell parameters extraction methods for solar PV system design and estimates and extracts unknown PV module parameters (I_{Ph}, I_D, R_s, R_{sh}, N₁) using such as SD, STM6 40/36, and STP6 120/36. The SCO was tested with 20 popular iterations per the CEC 2019 benchmark test function and compared to traditional optimization algorithms. RMSE values of the SCO algorithm are compared with those of other conventional algorithms such as GSK, DE, GOTLBO, RTLBO, and TLABC. Based on the compared findings, we may conclude that the SCO algorithm is an effective and trustworthy way of predicting the unknown optimized parameters of the solar PV module model under standard operating situations. Compared with other algorithms, the I-V and P-V characteristic curves and IAE results indicate that SCO can generate the optimized value of the estimated parameters for all the solar PV cell models. As a result, the close similarity between the generated I-V and P-V curves and the measured features has validated the SCO's accuracy. The statistical validity of the suggested algorithms has been examined using the Friedman and Wilcoxon tests. The focus areas include examining scalability, bolstering resilience in fluctuating situations, utilizing real-time controls, collaborating with machine learning, and developing specialized hardware. The fundamental SCO algorithm will be upgraded in the future to include parameter self-adapting methods to boost its performance while solving complex difficulties, as well as the MPPT problem action, the ANFSIS issue action and the hybrid optimisation technique will be used to find the optimal values of unknown parameters and RMS value.

REFERENCES

W. H. Bangyal, Z. A. Malik, I. Saleem, and N. U. Rehman, "An Analysis of Initialization Techniques of Particle Swarm Optimization Algorithm for Global Optimization," *4th Int. Conf. Innov. Comput. ICIC 2021*, no. Icic, 2021, doi: 10.1109/ICIC53490.2021.9692931.

- [2] Z. Yuan, J. Li, H. Yang, and B. Zhang, "A Hybrid Whale Optimization and Particle Swarm Optimization Algorithm," *Proc. 2021 IEEE Int. Conf. Prog. Informatics Comput. PIC 2021*, pp. 260–264, 2021, doi: 10.1109/PIC53636.2021.9687017.
- [3] M. F. Al-Hajri, K. M. El-Naggar, M. R. Al-Rashidi, and A. K. Al-Othman, "Optimal extraction of solar cell parameters using pattern search," *Renew. Energy*, vol. 44, pp. 238–245, 2012, doi: 10.1016/j.renene.2012.01.082.
- [4] A. Pahwa *et al.*, "Goal-Based Holonic Multiagent System for the Operation of Power Distribution Systems," *IEEE Trans. Smart Grid*, vol. 6, no. 5, pp. 2510–2518, 2015, doi: 10.1109/TSG.2015.2404334.
- [5] D. H. Muhsen, A. B. Ghazali, and T. Khatib, "Parameter extraction of a photovoltaic module using hybrid evolutionary algorithm," *2015 IEEE Student Conf. Res. Dev. SCORED 2015*, vol. 1, no. 1, pp. 533–538, 2015, doi: 10.1109/SCORED.2015.7449393.
- [6] S. Yahia, Y. Meraihi, A. Ramdane-Cherif, A. B. Gabis, D. Acheli, and H. Guan, "A Survey of Channel Modeling Techniques for Visible Light Communications," *J. Netw. Comput. Appl.*, vol. 194, no. September, 2021, doi: 10.1016/j.jnca.2021.103206.
- [7] M. A. Mughal, Q. Ma, and C. Xiao, "Photovoltaic cell parameter estimation using hybrid particle swarm optimization and simulated annealing," *Energies*, vol. 10, no. 8, pp. 1–14, 2017, doi: 10.3390/en10081213.
- [8] A. Sharma, A. Sharma, A. Moshe, N. Raj, and R. K. Pachauri, "An Effective Method for Parameter Estimation of Solar PV Cell Using Grey-Wolf Optimization Technique," *Int. J. Math. Eng. Manager. Sci.*, vol. 6, no. 3, pp. 911–931, 2021, doi: 10.33889/ijmems.2021.6.3.054.
- [9] O. S. Elazab, H. M. Hasanien, I. Alsaidan, A. Y. Abdelaziz, and S. M. Muyeen, "Parameter estimation of three diode photovoltaic model using grasshopper optimization algorithm," *Energies*, vol. 13, no. 2, 2020, doi: 10.3390/en13020497.
- [10] D. Oliva, A. A. Ewees, M. A. El Aziz, A. E. Hassanien, and M. P. Cisneros, "A chaotic improved artificial bee colony for the parameter estimation of photovoltaic cells," *Energies*, vol. 10, no. 7, pp. 1–19, 2017, doi: 10.3390/en10070865.
- [11] V. Stornelli, M. Muttillio, T. de Rubeis, and I. Nardi, "A new simplified five-parameter estimation method for single-diode model of photovoltaic panels," *Energies*, vol. 12, no. 22, 2019, doi: 10.3390/en12224271.
- [12] H. Al-Taani and S. Arabasi, "Solar irradiance measurements using smart devices: A cost-effective technique for estimation of solar irradiance for sustainable energy systems," *Sustain.*, vol. 10, no. 2, 2018, doi: 10.3390/su10020508.
- [13] C. Y. Park *et al.*, "Inverter efficiency analysis model based on solar power estimation using solar radiation," *Processes*, vol. 8, no. 10, pp. 1–19, 2020, doi: 10.3390/pr8101225.
- [14] A. Bocca *et al.*, "Multiple-regression method for fast estimation of solar irradiation and photovoltaic energy potentials over Europe and Africa," *Energies*, vol. 11, no. 12, pp. 1–17, 2018, doi: 10.3390/en11123477.
- [15] R. R. Ihsan, S. M. Almufti, B. M. Ormani, R. R. Asaad, and R. B. Marqas, "A Survey on Cat Swarm Optimization Algorithm," *Asian J. Res. Comput. Sci.*, no. July, pp. 22–32, 2021, doi: 10.9734/ajrcos/2021/v10i230237.
- [16] L. Li, G. Xiong, X. Yuan, J. Zhang, and J. Chen, "Parameter Extraction of Photovoltaic Models Using a Dynamic Self-Adaptive and Mutual-Comparison Teaching-Learning-Based Optimization," *IEEE Access*, vol. 9, pp. 52425–52441, 2021, doi: 10.1109/ACCESS.2021.3069748.
- [17] A. T. Kiani, M. Faisal Nadeem, A. Ahmed, I. A. Sajjad, A. Raza, and I. A. Khan, "Chaotic Inertia Weight Particle Swarm Optimization (CIWPSO): An Efficient Technique for Solar Cell Parameter Estimation," *2020 3rd Int. Conf. Comput. Math. Eng. Technol. Idea for Innov. Build. Knowl. Econ. iCoMET 2020*, 2020, doi: 10.1109/iCoMET48670.2020.9074085.
- [18] L. Zuo *et al.*, "Experimental research on the operation characteristics of solar chimney power plant combined with distillation (SCPPCD)," vol. 326, no. August, 2022, doi: 10.1016/j.apenergy.2022.120029.
- [19] M. A. El-Hameed, M. M. Elkholy, and A. A. El-Fergany, "Three-diode model for characterization of industrial solar generating units using manta-rays foraging optimizer: Analysis and validations," *Energy Convers. Manag.*, vol. 219, no. June, p. 113048, 2020, doi: 10.1016/j.enconman.2020.113048.
- [20] Q. Chen and X. Hu, "Design of intelligent control system for agricultural greenhouses based on adaptive improved genetic algorithm for multi-energy supply system," *Energy Reports*, vol. 8, pp. 12126–12138, 2022, doi: 10.1016/j.egyr.2022.09.018.
- [21] L. C. Borin, E. Mattos, R. Medke, C. R. D. Osorio, G. G. Koch, and V. F. Montagner, "Design of Robust Controllers Applied to DC-DC Converters with Uncertain Parameters Optimized by Metaheuristics," *2021 Brazilian Power Electron. Conf. COBEP 2021*, 2021, doi: 10.1109/COBEP53665.2021.9684008.
- [22] P. Kathirolu and K. Selvadurai, "Energy efficient cluster head selection using improved Sparrow Search Algorithm in Wireless Sensor Networks," *J. King Saud University - Comput. Inf. Sci.*, no. xxxx, 2021, doi: 10.1016/j.jksuci.2021.08.031.
- [23] H. Le Minh, T. Sang-To, M. Abdel Wahab, and T. Cuong-Le, "A new metaheuristic optimization based on K-means clustering algorithm and its application to structural damage identification," *Knowledge-Based Syst.*, vol. 251, p. 109189, 2022, doi: 10.1016/j.knosys.2022.109189.
- [24] F. Kiani, A. Seyyedabbasi, and P. Mahouti, "Optimal characterization of a microwave transistor using grey wolf algorithms," *Analog Integr. Circuit Signal Process.*, no. April 2022, 2021, doi: 10.1007/s10470-021-01914-y.
- [25] A. Hackl, C. Magele, and W. Renhart, "Extended firefly algorithm for multimodal optimization," *2016 19th Int. Symp. Electr. Appar. Technol. SIELA 2016*, no. 1, pp. 8–11, 2016, doi: 10.1109/SIELA.2016.7543010.